Supporting Information

Li$_2$RuO$_3$ as an Additive for High-Energy Lithium Ion Capacitors

Min-Sik Park,[†] Young-Geun Lim,[†] Jung-Woo Park,[†] Jeom-Soo Kim,[†,]* Jong-Won Lee,[‡]

Jung Ho Kim,[§] Shi Xue Dou,[§] and Young-Jun Kim[†,]*

[†] Advanced Batteries Research Center, Korea Electronics Technology Institute, 68 Yatap-dong, Bundang-gu, Seongnam 463-816, Republic of Korea.

[‡] New and Renewable Energy Research Division, Korea Institute of Energy Research, 152 Gajeong-ro, Yuseong-gu, Daejeon 305-343, Republic of Korea.

[§] Institute for Superconducting and Electronic Materials, University of Wollongong, North Wollongong, NSW2500, Australia.

Figure S1a and S1b shows FESEM images of Li_2MoO_3 and Li_2RuO_3 at low magnification, together with their particle size distributions (Figure S1c). Li_2MoO_3 has a slightly smaller average particle size ($D_{50} = 2.8$ µm) than Li_2RuO_3 does ($D_{50} = 3.1$ µm). Li_2MoO_3 has a wider particle size distribution and some large agglomerated particles, because residual carbon has remained on its surface as a result of carbothermal reduction during the powder-synthesis process.
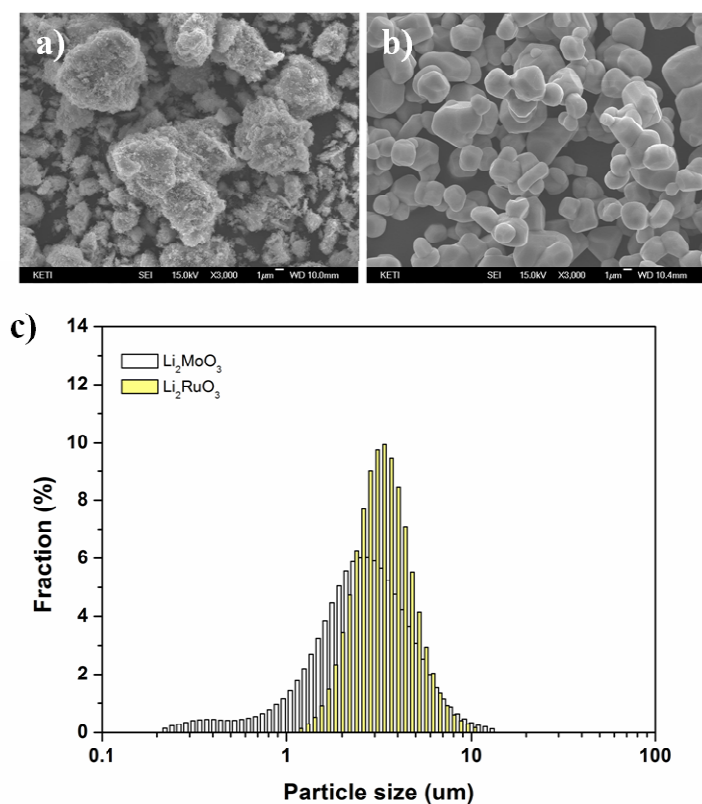

Figure S1. FESEM images of (a) Li_2MoO_3 and (b) Li_2RuO_3 at low magnification; (c) a comparison of the particle size distributions for Li_2MoO_3 and Li_2RuO_3; average particle sizes for Li_2MoO_3 and Li_2RuO_3 were estimated to be $D_{50} = 2.8$ µm and $D_{50} = 3.1$ µm, respectively.

The current electrolyte could be decomposed by high-voltage charging above 4.3 V (*vs.* Li/Li^+) for Li^+ pre-doping, which might affect the delivered capacity of Li_2RuO_3. To clarify the effects of electrolyte decomposition on the charge capacity of Li_2RuO_3, we systematically

investigated the electrochemical properties of Li_2RuO_3 using a four-electrode cell, configured as Li | Li_2RuO_3 | $Li_4Ti_5O_{12}$ | Li. First, Li_2RuO_3 electrode and $Li_4Ti_5O_{12}$ electrode were set as working and counter electrodes, respectively. The Li electrode was used as a reference electrode for monitoring Li^+ extraction from the Li_2RuO_3 electrode and Li^+ insertion into the $Li_4Ti_5O_{12}$ electrode. After the first charging to various cut-off voltages (4.1, 4.3, 4.5, 4.7, and 5.0 V *vs.* Li/Li^+), the $Li_4Ti_5O_{12}$ electrode was set as a working electrode and another Li electrode was set as counter and reference electrode for Li^+ extraction from the $Li_4Ti_5O_{12}$ electrode.

The additional capacity due to the electrolyte decomposition can be estimated from the difference between achieved capacities at high cut-off voltages (4.3, 4.5, 4.7 and 5.0 V *vs.* Li/Li^+) and the capacity obtained from Li_2RuO_3 by charging to the moderate voltage of 4.1 V (*vs.* Li/Li^+). To exclude the influence of undesirable side reactions originating from the corresponding electrodes, the $Li_4Ti_5O_{12}$ electrode was employed as a counter electrode. $Li_4Ti_5O_{12}$ features a sufficiently high flat-voltage plateau at 1.55 V (*vs.* Li/Li^+) that prevents reduction of electrolyte, in which the charge consumed by passivation film formation on the surface of electrodes may be neglected. The $Li_4Ti_5O_{12}$ electrodes exhibit a direct dependence on capacity at different charge cut-off voltages. These are favorable for use as counter electrodes for the quantification of the capacity without undesirable side reactions.

Li^+ was successfully delivered to the $Li_4Ti_5O_{12}$ counter electrode by charging Li_2RuO_3 to 4.1 V (*vs.* Li/Li^+) as shown in Figure S2a. As charge voltage increases, the amount of Li^+ extraction (charge capacity) from Li_2RuO_3 also increases. As a result, the charge capacities for Li^+ insertion to $Li_4Ti_5O_{12}$ increased accordingly. After that, the $Li_4Ti_5O_{12}$ electrode was set as a working electrode and then discharged to 1.5 V (*vs.* Li/Li^+) over a Li counter electrode (Figure S2b). The estimated amount of Li^+ extracted (discharge capacity) from $Li_4Ti_5O_{12}$ is considered to be the same as that of Li^+ extracted from Li_2RuO_3, after careful

analysis of the initial coulombic efficiency of $Li_4Ti_5O_{12}$, as described in Figure S2c. For practical estimation, we should take into account the initial coulombic efficiency of $Li_4Ti_5O_{12}$ (92.0%).

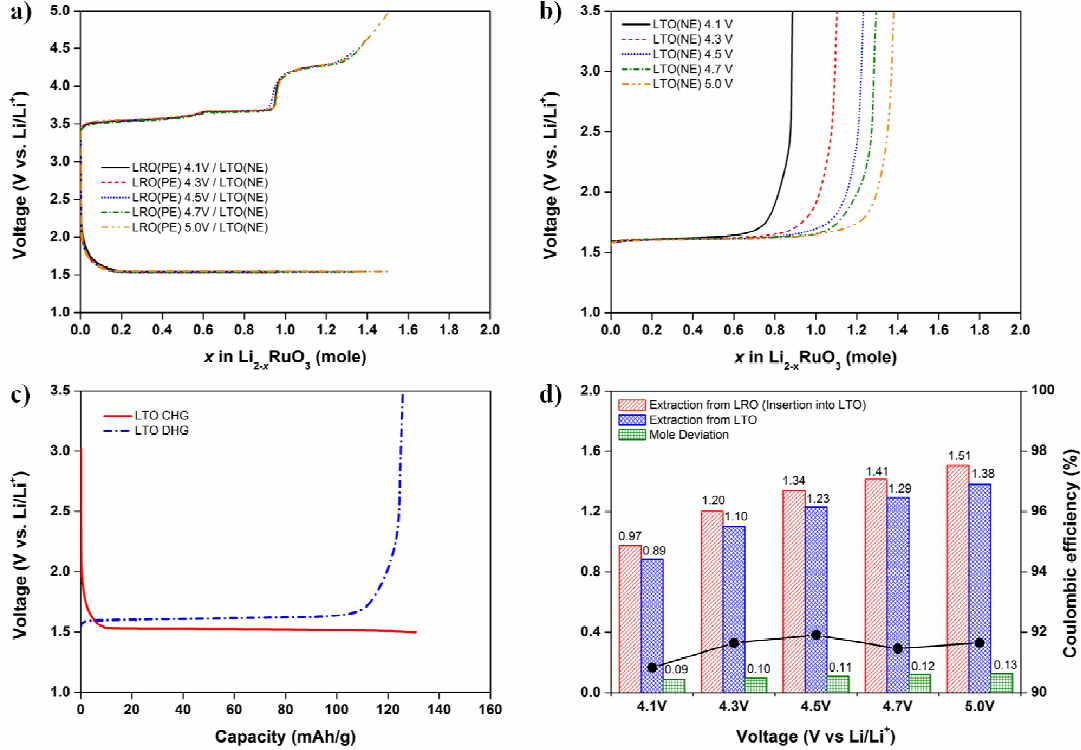**Figure S2.** (a) Comparisons of charge capacities of Li_2RuO_3 and $Li_4Ti_5O_{12}$ measured at different cut-off voltages, such as 4.1, 4.3, 4.5, 4.7, and 5.0 V *vs.* Li/Li$^+$, and (b) subsequent discharge capacities of $Li_4Ti_5O_{12}$ measured with a Li counter electrode. (c) galvanostatic charge and discharge profiles of $Li_4Ti_5O_{12}$ measured with a Li counter electrode, and (d) a summary of the estimated capacities due to the electrolyte decomposition at different charge cut-off voltages.

Results of the measurements carried out at different charge cut-off voltages are summarized in Figure S2d. According to the comparison, the amount of Li$^+$ (charge capacity) extracted from Li_2RuO_3 was estimated to be 0.97 mol, whereas the amount of Li$^+$ extracted

(discharge capacity) from $Li_4Ti_5O_{12}$ is about 0.89 mol after charging to 4.1 V (*vs.* Li/Li$^+$). The capacity loss was calculated to be about 0.09 mol. If it is assumed that the current electrolyte did not decomposed at 4.1 V (*vs.* Li/Li$^+$), then the capacity loss could be introduced by initial irreversibility of $Li_4Ti_5O_{12}$. After charging to higher charge cut-off voltages, we conducted the same estimations. When Li_2RuO_3 was charged to 4.7 V (*vs.* Li/Li$^+$), the difference was about 0.12 mol, which indicates that the capacity arising from the electrolyte decomposition is 0.03 mol. As for charging to 5.0 V (*vs.* Li/Li$^+$), the estimated capacity due to the electrolyte decomposition is about 0.04 mol. In conclusion, the effect of electrolyte decomposition is not significant at least during the first charge.
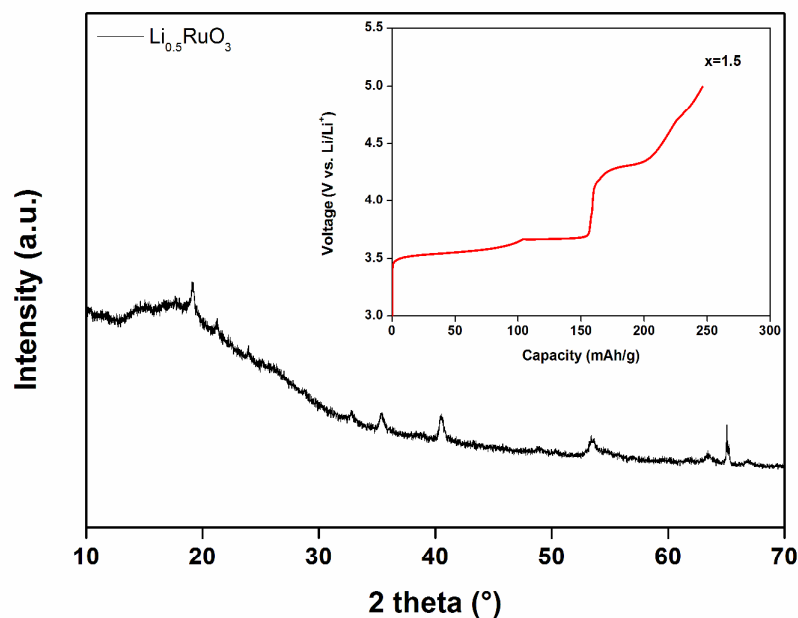

Figure S3. Capacity-voltage plot (inset) and corresponding *ex-situ* X-ray diffraction (XRD) patterns for $Li_{2-x}RuO_3$ (*x* = 1.5) electrode when the cell was charged up to 5.0 V *vs.* Li/Li$^+$.
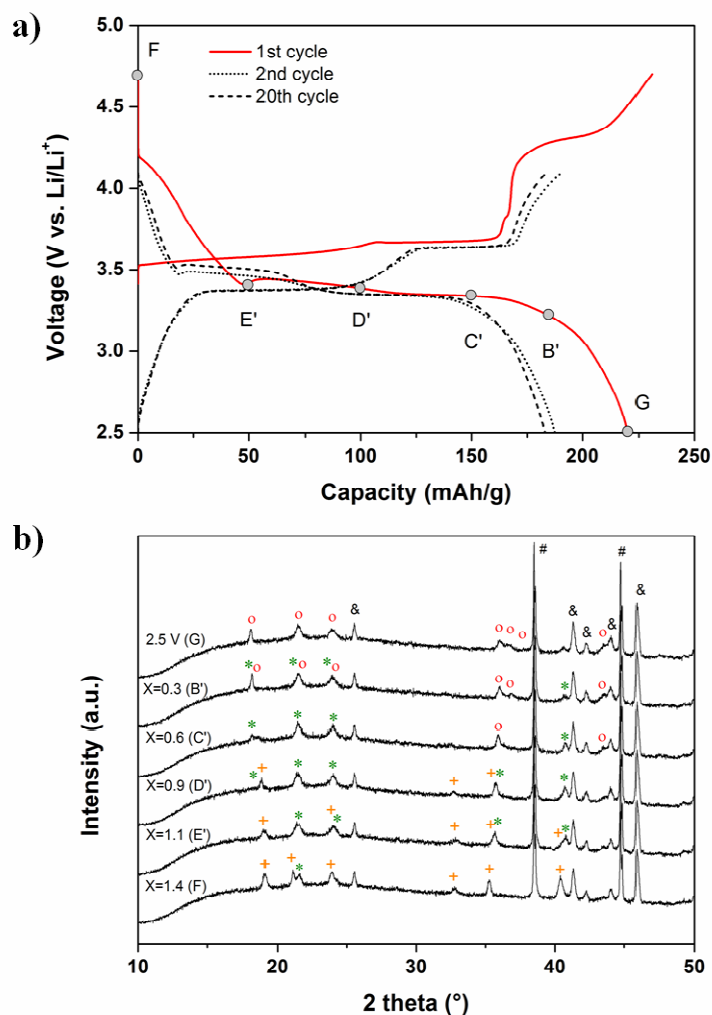
Figure S4. (a) Galvanostatic charge and discharge profiles for Li_2RuO_3 in the voltage range of 2.5 - 4.7 V for the first cycle (solid-line) and in the voltage range of 2.5 - 4.1 V for the second (dot-line) and twentieth cycles (dash-line); (b) in-situ XRD patterns collected at different SOCs ($Li_{2-x}RuO_3$, x = 0, 0.3, 0.6, 0.9, 1.1, 1.4) during the first discharge and discharge, marked with Li_2RuO_3 (o), $Li_{1.4}RuO_3$ (*), and $Li_{0.9}RuO_3$ (+) references.

Figure S3 shows the *ex situ* XRD patterns for $Li_{2-x}RuO_3$ (x = 0.5) after charging to 5.0 V (*vs.* Li/Li^+). According to the result of the *ex-situ* XRD measurement, further structural change from $Li_{0.9}RuO_3$ with a rhombohedral symmetry does not occur even after 1.5 mol of Li^+ is electrochemically extracted. In our research, the lithium ion capacitor (LIC) was

charged to 4.7 V (*vs.* Li/Li$^+$) initially for supplying Li$^+$ to the NE. Approximately 1.4 mol of Li was extracted from Li$_2$RuO$_3$ during this process. Beyond 4.3 V, the Bragg peaks shift to higher 2θ-positions as the charge voltage increases, without accompanying formation of other phases. *In situ* XRD results for the Li$_2$RuO$_3$ electrode during the subsequent discharge are presented in Figure S4. We confirm that all reflections were reversibly restored to the original state.
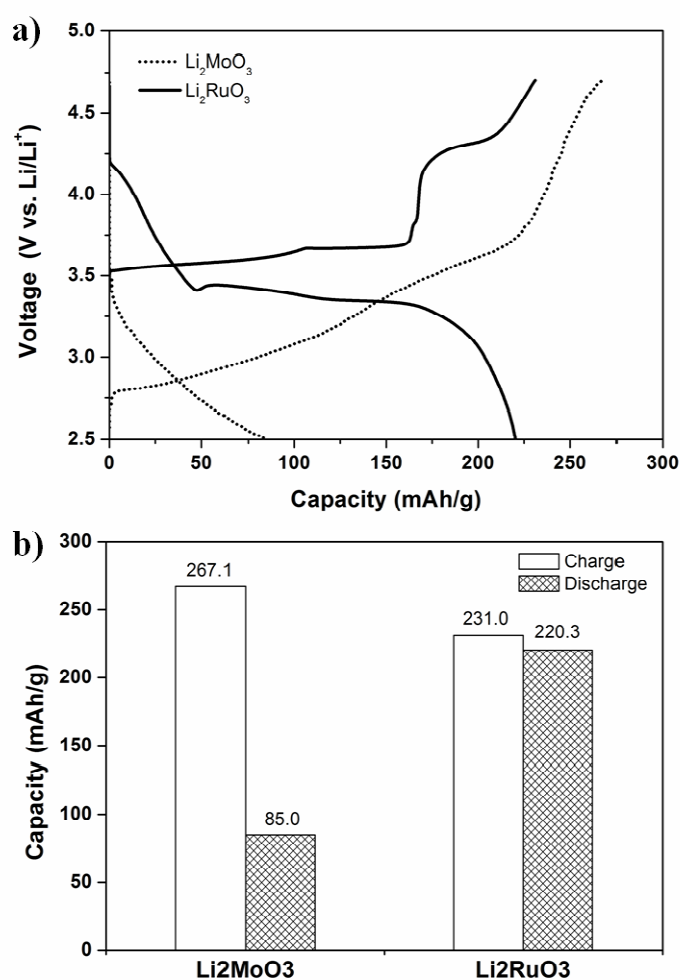

Figure S5. (a) Galvanostatic charge and discharge profiles for Li$_2$MoO$_3$ (dot-line) and Li$_2$RuO$_3$ (solid-line) at the first cycle (0.1 C, 2.5 - 4.7 V *vs.* Li/Li$^+$); (b) comparison of charge and discharge capacities for Li$_2$MoO$_3$ and Li$_2$RuO$_3$ at the first cycle.

For comparative purposes, the amount of activated carbon and Li_2MoO_3 in the PEswere fixed at 5.81 and 2.24 mg, respectively. The amounts of Li_2RuO_3 were controlled at 0, 5, and 10 wt%, respectively, to evaluate the influence of the addition of Li_2RuO_3 on the electrochemical properties of the LIC. More detailed information, including the loading level and density of the PEs, is given in Table S1.

Table S1. Detailed information on the composition of the positive electrodes.

Cathode	Activated carbon (mg)	Li_2MoO_3 (mg)	Li_2RuO_3 (mg)	PVDF (mg)	Total		
					Mass (mg)	Loading (mg/cm^2)	Density (g/cm^3)
Metallic Li	5.81 (92 wt%)	- -	- -	0.5 (8 wt%)	6.31 (100 wt%)	5.6	0.5
Li_2MoO_3	5.81 (66.4 wt%)	2.24 (25.6 wt%)	- -	0.70 (8 wt%)	8.74 (100 wt%)	7.7	0.5
Li_2RuO_3- 5wt%	5.81 (62.8 wt%)	2.24 (24.2 wt%)	0.46 (5 wt%)	0.74 (8 wt%)	9.25 (100 wt%)	8.2	0.5
Li_2RuO_3- 10wt%	5.81 (59.2 wt%)	2.24 (22.8 wt%)	0.98 (10 wt%)	0.79 (8 wt%)	9.81 (100 wt%)	8.7	0.5

Figure S5 shows galvanostatic charge and discharge profiles for Li_2MoO_3 and Li_2RuO_3. CR2032 coin-type half cells were assembled to characterize the electrochemical properties of metal oxide additives with Li metal as the counter and reference electrode. The cells were initially charged up to 4.7 V (*vs.* Li/Li$^+$) to supply Li$^+$ during the lithium-doping process and then discharged to 2.5 V (*vs.* Li/Li$^+$). Based on the obtained electrochemical results, we optimized the positive electrode (PE) and calculated the exact amounts of the various

components in the PEs, such as activated carbon, Li_2MoO_3, and Li_2RuO_3. The irreversible capacity of Li_2MoO_3, which was found to be 182.2 mAh/g, could be used as a lithium source for lithium doping of the NE. On the other hand, the electrochemical Li^+ insertion and extraction are highly reversible in Li_2RuO_3, which could provide more electrochemical energy to the cell when it is employed in the PE of the LIC.
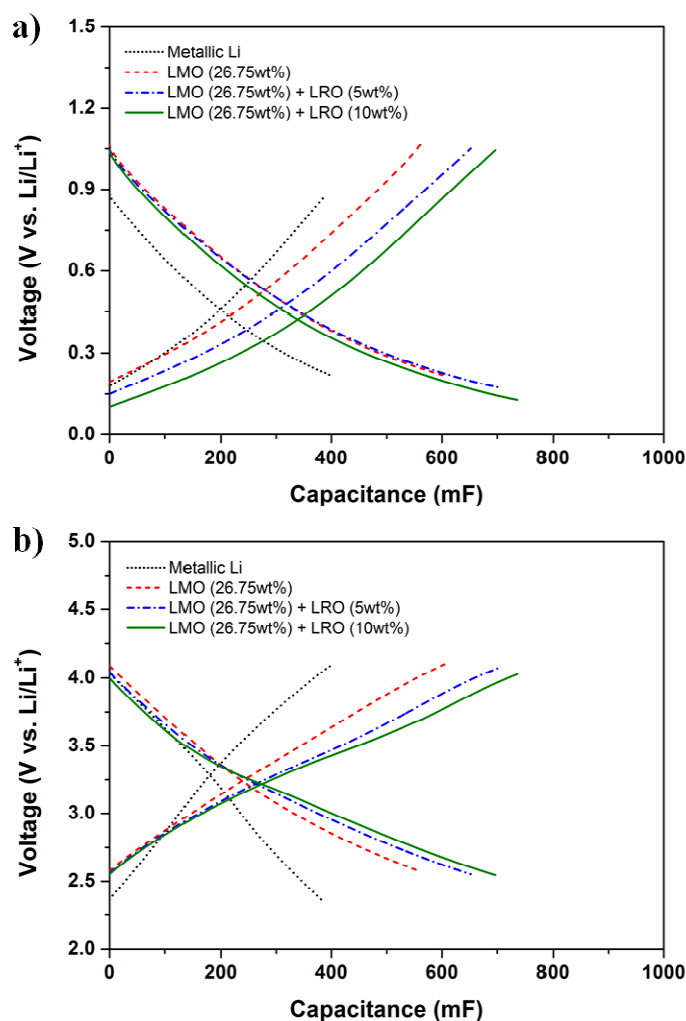

Figure S6. (a) NE voltage profiles and (b) PE voltage profiles for the LICs including different amounts of Li_2RuO_3 in the cathode during charge and discharge in the voltage range of 1.5 to 3.9 V with a constant current density of 5.3 mA/g (0.1 C). A LIC conventionally doped with metallic lithium is included as a reference.

To verify the practical process of lithium doping, the cells were initially charged up to 4.7 V (*vs.* Li/Li$^+$) and then discharged to 2.5 V (*vs.* Li/Li$^+$). The cells were subsequently cycled in the voltage range of 2.5 to 4.1 V (*vs.* Li/Li$^+$), corresponding to the practical operating voltage range of the PE in the LIC full cells. After the lithium doping process, Li$_2$RuO$_3$ reacted reversibly and produced a plateau in the voltage range of 3.0 to 3.5 V (*vs.* Li/Li$^+$). This contributes to the capacity of about 180 mAh/g. Figures S6a and S6b show voltage profiles during charge and discharge of the NEs and PEs, for the LIC full cells respectively, and the different amounts of Li$_2$RuO$_3$ in the PE. The full cells were cycled in the voltage range of 1.5 to 3.9 V at a constant current density of 5.3 mA/g (0.1 C). A plateau was reached at voltages of around 3.5 V. This originated from the electrochemical activity of the Li$_2$RuO$_3$ additive in the PE of the LIC full cell. This implies that Li$_2$RuO$_3$ reversibly participates in the electrochemical reaction in the PE and provides additional capacitance.

Figure S7 shows voltage profiles of NEs measured from the LIC full cells in the four-electrode configuration during cycling. The LIC prepared by the metallic lithium doping method shows distinctive behavior on charging (Figure S6a) and discharging (Figure S6b), in which the NE voltage is gradually increased upon cycling. This behavior is more clearly observed on discharging (Figure S6b). During discharge, the NE voltage of the LICs should not change much while the PE voltage decreases to maximize the energy. Under the same design conditions, the voltage increase of the NE during cycling is an unfavorable phenomenon. Such an increase could be attributed to the reduction in the available amount of Li$^+$ that participates in the electrochemical reaction in the NE. In contrast, the LICs containing metal oxides as additives exhibited more stable voltage profiles during cycling.
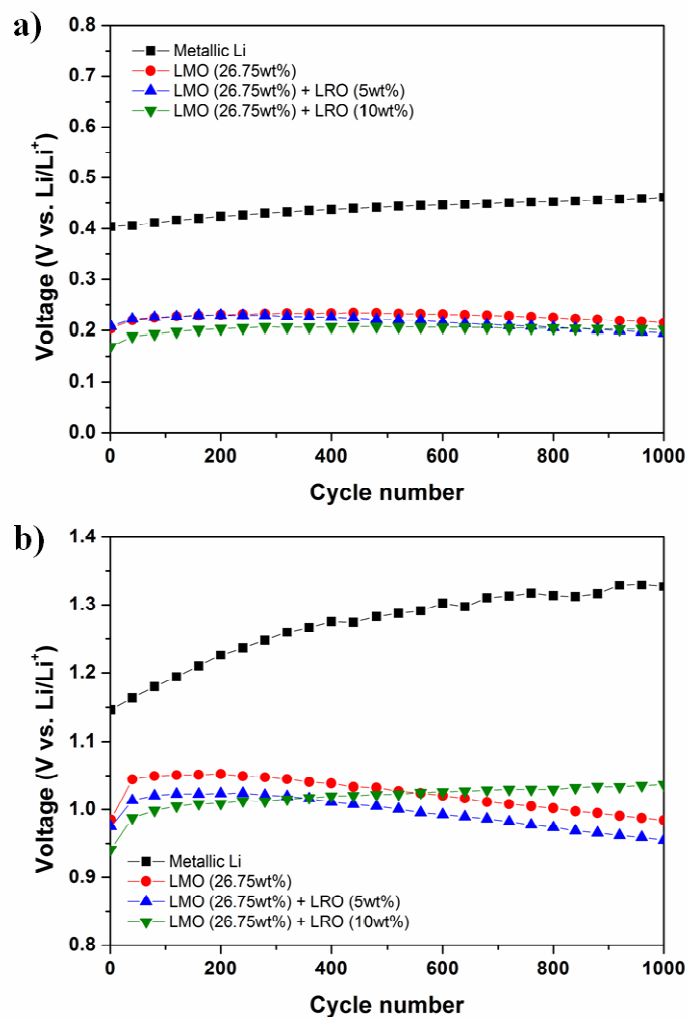
Figure S7. Voltage profiles of NEs in the LICs during cycling (10 C, 1.5 - 3.9 V): (a) charge and (b) discharge.